



ARTICLE

Open Access



# Assessment of iridoid profiles in the growth period of aerial parts of *Pseudolysimachion rotundum* var. *subintegrum* and their antioxidant and MUC5AC inhibitory potential

Soobin Song<sup>1†</sup>, Doo-Young Kim<sup>1†</sup>, Seon Min Oh<sup>1†</sup>, So-Yeun Woo<sup>1</sup>, Il-joo Kim<sup>1</sup>, Mun-Ock Kim<sup>1</sup>, Ji-Yoon Park<sup>1</sup>, Namho Kim<sup>1</sup>, Hae-Young Kim<sup>1</sup>, Juhee Lee<sup>2</sup>, Sang Yoon Kim<sup>2</sup>, Bang Yeon Hwang<sup>3\*</sup>, Hyung Won Ryu<sup>1\*</sup>  and Sei-Ryang Oh<sup>1\*</sup> 

## Abstract

YPL-001 is a drug substance of *Pseudolysimachion rotundum* var. *subintegrum* and has been reported to be a potent COPD inhibitor. For the first time, this study demonstrated a correlation among the iridoid constituents, antioxidants, and MUC5AC inhibition activities in *P. rotundum* during different growth stages (5 to 11 weeks). Single-factor extraction was used to optimize the plant extraction conditions to maximize the major iridoid constituents (70% ethanol, 40 °C, 1 h); isolated metabolites 1–6 were identified using nuclear magnetic resonance spectroscopy (NMR) and mass spectrometry (MS). The contents of each metabolite and antioxidant/MUC5AC inhibition effects were markedly changed according to the growth stages, especially for catalposide (2, 5.97 → 10.99 mg/g, 1.8-fold) and isovanillyl catapol (5, 4.42 → 20.00 mg/g, 4.5-fold), which were the predominant substances in August. Our results indicated that YPL-001 could potentially contribute to enhancing the *P. rotundum* value in accumulated iridoids at the growth stage and the biological effect aspects to develop industrial medicinal crops.

**Keywords** *Pseudolysimachion rotundum* var. *Subintegrum*, Growth stages, Quality control, Antioxidant, MUC5AC

<sup>†</sup>Soobin Song, Doo-Young Kim and Seon Min Oh are contributed equally to this work.

\*Correspondence:  
Bang Yeon Hwang  
byhwang@chungbuk.ac.kr  
Hyung Won Ryu  
ryuhw@kribb.re.kr  
Sei-Ryang Oh  
seiryang@kribb.re.kr

<sup>1</sup> Natural Product Research Center, Korea Research Institute of Bioscience and Biotechnology, Cheongju-si, Chungcheongbuk-do 28116, Republic of Korea

<sup>2</sup> Department of Agricultural Chemistry & Interdisciplinary Program in IT-Bio Convergence System, Suncheon National University, Suncheon-si, Jeollanam-do 57922, Republic of Korea

<sup>3</sup> College of Pharmacy, Chungbuk National University, Cheongju-si, Chungcheongbuk-do 28160, Republic of Korea

## Introduction

*Pseudolysimachion rotundum* var. *subintegrum*, belonging to the Plantaginaceae family, grows in many parts of Korea, China, Russia, and Europe but is abundant in Korea [1]. The species is well known for its high content of iridoid glycoside compounds, including picroside C, verproside, isovanillyl catapol, picroside II, 6-O-veratroyl catapol, and catalposide, which are related to biological effects such as anti-inflammation [2], anti-asthma [3], anti-COPD [4], and anticancer [5]. Their iridoid glycoside compounds were investigated for their high anti-inflammatory properties. The six iridoids were then selected to constitute a drug candidate mixture that was named YPL-001, which was developed as a natural drug by Yungjin Pharm. Co., Ltd. YPL-001 showed good efficacy in reducing airway inflammation

in human lung cell lines and in a mouse model of asthma. YPL-001 successfully completed Clinical Trial Phase 2a (ClinicalTrials.gov identifier: NCT02272634, USA) as a potent therapeutic agent against COPD (<https://clinicaltrials.gov/ct2/show/NCT02272634?term=NCT02272634&draw=2&rank=1>, accessed 01.25.23). A previous study reported phytochemicals in the chemical composition of *P. rotundum*, including plant extracts and YPL-001. However, few studies have reported phytochemical changes through growth stage properties in the aerial parts of *P. rotundum*.

Plant phytochemical properties and content at the optimal stage of maturity have a significant impact on dry weight, quality and biological activity [6]. First, abiotic factors such as temperature extremes, drought, flooding, salinity, and heavy metal stress are major yield-limiting factors because they affect plant crop growth and yield formation [7]. Therefore, plant quality control can be attributed to growth changes according to maturation and growth stages and responses to microclimates such as temperature, precipitation, and humidity of crops in the cultivated environment [8]. Second, each of these biotic factors includes plants, animals, fungi, and bacteria that directly or indirectly affect each of the other organisms in an ecosystem through various types of interactions [9]. Therefore, in recent years, this aspect has been considered from the beginning to the final stage of CMC (chemistry, manufacturing, control) of botanical raw material and drug substances in drug development using natural materials. Metabolic analysis related to the ripening and growth stages of plants using GC-MS, LC-MS, NMR, and combination tools in the CMC strategy can aid in the understanding of phytochemical diversity [10–16].

The aim of this study was to compare the metabolome profile of this plant during the flowering period of July–August, which has the most ornamental value during the growth phase, and to elucidate the bioactive iridoid glycoside metabolites. Through multivariate data analyses such as principal component analysis (PCA), orthogonal partial least squares discriminant analysis (OPLS-DA), and S-plot using ultraperformance liquid chromatography coupled with Q-TOF mass spectrometry (UPLC-Q-TOF/MS), variations in the metabolite profiles of the aerial parts of *P. rotundum* were investigated. In addition, *P. rotundum* extracts during growth stages were evaluated to confirm simple antioxidant activities and MUC5AC inhibitory effects. Based on our results, we expect to be able to determine the optimal harvesting stage for industrially available drug substances from the aerial parts of *P. rotundum*.

## Materials and methods

### Plant materials

The seeds of *Pseudolysimachion rotundum* var. *subintegrum* were provided by Dr. Jeong Hoon Lee [Department of Herbal Crop Research, National Institute of Horticultural and Herbal Science (NIHHS), RDA] in September 2020 and were cultivated and collected in a well-controlled glass greenhouse at the KRIBB, Cheong-ju, Korea. The plant was reidentified at IBMRC, KRIBB, and deposited KRIBB as a voucher specimen (KRIB 0020697). The soil type (pH, organic matter, electrical conductivity, and soil classification) and climate condition (average and/or min-max temperatures, humidity, rain, etc.) for cultivation consisted of the area in which the plant material is present as described in Additional file 1: Table S1 (Eco-Friendly Agriculture Center, Sunchon National University). The seeds were distributed over a seeding tray (50 holes, 54×28 cm, 4.5×4.5×5.0 cm/hole, 70 cc/hole) at a density of 3–4 seeds per pot. Five weeks after germination, the plants were transplanted to an open field in KRIBB (36°43′12.6″ N 127°26′1.6″ E). The dates for germination and transplantation were May 3, 2021, and June 7, 2021, respectively. The plants were harvested once every 2 weeks over a period of 2 months: July 15, 2021, (5th week after transplant) up to August 26, 2021, (13th week after transplant) (Additional file 1: Table S2). Collected plants were rapidly lyophilized, ground, and stored sealed at –20 °C for 15 weeks for analysis.

### Instruments and chemicals

High-speed countercurrent chromatography (HSCCC) was carried out with a TBE-1000 A high-speed countercurrent chromatography system (Shanghai Tauto Biotech Co. Ltd., Shanghai, China) with three serially connected multilayer coil separation columns and an 80 mL line. The system was equipped with an LPLC pump (TBP5002, Shanghai Tauto Biotech Co. Ltd., Shanghai, China), an SSI 500 UV detector (Thermo Electron Co., San Jose, CA), and the Autochro-WIN program (version 3.0, Younglin-Tech, Seoul, Korea). NMR spectra were measured on a Bruker AM500 instrument (Billerica, Massachusetts, USA). Organic solvents (HPLC grade) from Merck (Darmstadt, Germany), formic acid from Sigma-Aldrich (St. Louis, MO, USA), and NMR solvents from Cambridge Isotope Lab Inc. (Andover, MA, USA) were purchased and used. Ultra-pure water was prepared using a purification system (Milli-Q Academic, Merck Millipore).

### Sample extraction

A total of 500 mg of a dry pulverized sample of the aerial parts of *P. rotundum* was weighed, 10 mL of 10, 30, 50, 70, and 95% ethanol (EtOH) was added, the sample was extracted three times at room temperature over a 2 h period, and the experiment was repeated 5 times for each concentration. The supernatant was filtered through Whatman filter paper No. 1, and the filtered extract was concentrated using a fully automatic high-speed rotary concentrator (Biotage V10-Touch). The weight was measured to calculate the yield. The extract was centrifuged, HPLC analysis was performed with 1 mL of the supernatant, and the relative content of verproside was compared to confirm the optimal solvent conditions. A total of 500 mg of a dry pulverized sample of *P. rotundum* was weighed, 10 mL of 70% EtOH was added, the sample was placed in a water bath at 25, 30, 40, 50, 70, and 90 °C and extracted three times over a 2 h period, and the experiment was repeated 5 times for each concentration. To check the temperature and time conditions, extraction was performed under 70% EtOH conditions in a 25, 30, 40 °C water bath, and the extraction time was 1, 2, 4, 6 h. Filtration and concentration of the extract were performed under the same conditions as in the experiment under the optimal solvent conditions.

### Data processing and multivariate analysis

Analysis was performed on an I-Class (Waters Corp., Milford, MA, USA) instrument equipped with a BEH C18 column. The column oven was set at 35 °C, and the tray was at 4 °C. The mobile phase used for the analysis was commonly used A (0.1% FA in water (v/v)) and B (0.1% FA (v/v) in acetonitrile). For analysis, the flow rate was 0.4 mL/min, and the sample injection volume was 2 µL. The solvent composition for UPLC was as follows: 0–1 min, 5% B; 1–20 min, 100% B; 20–22.3 min, 100% B; 22.3–22.4 min, 5% B; and 22.4–25 min, 5% B. Mass spectrometry (anion and cation modes) was analyzed using a Xevo G2-S (Waters Corp., Milford, MA, USA). The detailed MS analysis conditions were set as follows: 3.0 kV capillary, 110 °C source temperature, 40 V cone voltage, 50 L/h cone gas flow, 350 °C desolvation temperature, and 800 L/h desolvation gas flow. Accurate mass measurements were obtained with an automatic calibrated delivery system using an internal standard (leucine-enkephalin).

All MS<sup>E</sup> results collected by analysis were processed through the UNIFI program (Waters Corp., Milford, USA). MS<sup>E</sup> results were processed through a vertex-peak detection and alignment algorithm and analyzed with Progenesis QI software. (Waters Corp, Milford, USA). The intensity of each ion was calculated as the peak area by normalizing the total ion count to the retention time

and *m/z* value to generate a data matrix. To perform multivariate statistical analysis, three-dimensional data composed of RT-*m/z* pair, name, and areas were converted to the EZinfo program (UMETRICS). Metabolites were aligned, and peak areas were normalized and exported to SIMCA-P+ 12.0 (Umetrics, Umeå, Sweden) for multivariate analysis. The data were mean-centered and Pareto-scaled before PCA, PLS-DA, and OPLS-DA.

### Extraction and isolation of phytochemicals

The dried aerial parts of *P. rotundum* (2.0 kg) were immersed in CH<sub>3</sub>OH (10 L, × 3) at room temperature, and the solvent was concentrated using an evaporator under reduced pressure at 40 °C to obtain the methanolic extract (198.7 g). A portion of the methanolic extract (30 g) was subjected to C18 column chromatography using MeOH-H<sub>2</sub>O (3:97, 25:75, 65:35, 100:0 v/v) to give four fractions (PL-1 to PL-4). Fraction PL3 (5 g) was further fractionated by medium-pressure liquid chromatography (MPLC) with an RP C-18 column (5 × 49 cm, 40C<sub>18</sub>-prep) eluted with MeOH-H<sub>2</sub>O (20:80, 30:70, 40:60 v/v, *step gradient*) to provide five fractions (PL3m-1 to PL3m-5). Fraction PL3m-1 (1.2 g) was subjected to preparative HPLC using MeOH-H<sub>2</sub>O (1:2, v/v) to produce compound 1 (500 mg). Fraction PL3m-2 (800 mg) was purified by Sephadex LH-20 (2.5 × 170 cm) column chromatography eluted with 90% MeOH to give four subfractions, PL3m-2-1 to PL3m-2-4. Subfraction PL3m-2-1 (52.6 mg) was purified by prep-HPLC using an Atlantis<sup>®</sup> T<sub>3</sub> column (5 µm particle size, 19 × 250 mm; mobile phase of 18% ACN in H<sub>2</sub>O; flow rate of 16 mL/min; UV detection at 263 nm] to obtain compound 2 (12.5 mg). Compounds 3 (19.7 mg) and 5 (28.7 mg) were obtained from the purification of a portion of fraction PL3m-4 (2.8 g) by HSCCC [*n*-BuOH/H<sub>2</sub>O=1:1 v/v, upper phase for the stationary phase, lower phase for the mobile phase; loading sample: 100 mg; flow rate: 5.5 mL/min; 600 rpm; forward; UV: 263 nm]. Fraction PL3m-4 (18.3 mg) was isolated by preparative HPLC [Atlantis<sup>®</sup> prep T<sub>3</sub> OBD<sup>™</sup> column (5 µm particle size, 19 × 250 mm); mobile phase 18% ACN in H<sub>2</sub>O; flow rate 16 mL/min; UV detection at 263 nm] to give compound 4 (5.4 mg). Fraction PL3m-5 (50.6 mg) was further separated with an RP-C18 MPLC column eluting with a gradient of MeOH-H<sub>2</sub>O (4:6, 5:5, 6:4, 7:3, 10:0) to produce compound 6 (1.9 mg).

### Verproside (1)

The characteristics of verproside (1) are as follows: white amorphous powder; m.p. 145–150 °C; [α]<sub>D</sub><sup>20</sup> -153.7° (*c* 0.1, CH<sub>3</sub>OH); HRESIMS (negative) *m/z* 497.1366 [M-H]<sup>-</sup>, calcd for C<sub>22</sub>H<sub>25</sub>O<sub>13</sub> 497.1354. <sup>1</sup>H NMR (400 MHz, DMSO-*d*<sub>6</sub>) δ<sub>H</sub> 2.46 (1 H, d, *J*=8.4, H-9), 2.59 (1 H, dddd, *J*=1.6, 4.0, 8.0, 8.0, H-5), 3.00 (1 H, m, H-G4),

3.05 (1 H, m, H-G2), 3.14 (1 H, m, H-G5), 3.18 (1 H, m, H-G3), 3.42, 3.71 (2 H, m, H-G6), 3.67 (1 H, s, H-7), 3.71, 3.91 (2 H, d,  $J=13.2$  Hz, each, H-10), 4.61 (1 H, d,  $J=7.6$  Hz, H-G1), 4.94 (1 H, dd,  $J=4.0, 6.0$  Hz, H-4), 5.03 (1 H, d,  $J=8.0$  Hz, H-6), 5.09 (1 H, d,  $J=9.2$  Hz, H-1), 6.41 (1 H, d,  $J=5.6$  Hz, H-3), 6.82 (1 H, d,  $J=8.0$  Hz, H-5'), 7.35 (1 H, dd,  $J=2.0, 8.0$  Hz, H-6'), 7.39 (1 H, d,  $J=2.0$  Hz, H-2') [17].

#### Catalposide (2)

The characteristics of catalposide (2) are as follows: crystalline needles; m.p. 215–216 °C;  $[\alpha]_D^{20}$  -166.0° ( $c$  0.58, CH<sub>3</sub>OH); HRESIMS (negative)  $m/z$  481.1327 [M-H]<sup>-</sup>, calcd for C<sub>22</sub>H<sub>25</sub>O<sub>12</sub> 481.1346. <sup>1</sup>H-NMR (400 MHz, DMSO-*d*<sub>6</sub>)  $\delta_H$  2.47 (1 H, dd,  $J=8.0, 9.6$  Hz, H-9), 2.56 (1 H, dddd,  $J=1.2, 4.0, 8.0, 8.0$  Hz, H-5), 3.00 (1 H, m, H-G4), 3.05 (1 H, m, H-G2), 3.14 (1 H, m, H-G5), 3.18 (1 H, m, H-G3), 3.43, 3.72 (2 H, m, H-G6), 3.69 (1 H, br s, H-7), 3.72, 3.92 (2 H, d,  $J=13.2$  Hz, each, H-10), 4.62 (1 H, d,  $J=8.0$  Hz, H-G1), 4.96 (1 H, dd,  $J=4.0, 6.0$  Hz, H-4), 5.05 (1 H, dd,  $J=1.2, 8.0$  Hz, H-6), 5.11 (1 H, d,  $J=9.6$  Hz, H-1), 6.42 (1 H, dd,  $J=1.2, 6.0$  Hz, H-3), 6.86 (2 H, d,  $J=8.0$  Hz, H-3', 5'), 7.85 (2 H, d,  $J=2.0$  Hz, H-2', 6') [17].

#### Picroside II (3)

The characteristics of picroside II (3) are as follows: light brownish powder; m.p. 137–140 °C;  $[\alpha]_D^{20}$  -158.7° ( $c$  0.11, CH<sub>3</sub>OH); HRESIMS (negative)  $m/z$  511.1475 [M-H]<sup>-</sup>, calcd for C<sub>22</sub>H<sub>27</sub>O<sub>13</sub> 511.1604. <sup>1</sup>H-NMR (400 MHz, DMSO-*d*<sub>6</sub>)  $\delta_H$  5.11 (d,  $J=9.3$  Hz, H-1), 6.42 (d,  $J=5.8$  Hz, H-3), 4.97 (dd,  $J=5.8, 4.4$  Hz, H-4), 2.58 (dd,  $J=9.3, 7.6$  Hz, H-5), 5.06 (d,  $J=7.6$  Hz, H-6), 3.67 (br s, H-7), 2.47 (d,  $J=9.3$  Hz, H-9), 3.72 (m, H-10), 3.93 (d,  $J=13.2$  Hz, H-10), 7.46 (s, H-2'), 6.85 (d,  $J=7.6$  Hz, H-5'), 7.52 (d,  $J=7.6$  Hz, H-6'), 4.63 (d,  $J=7.6$  Hz, H-Glc-1''), 3.07 (dd,  $J=8.0, 7.6$  Hz, H-Glc-2''), 3.18 (m, H-Glc-3''), 3.03 (m, H-Glc-4''), 3.14 (m, H-Glc-5''), 3.44 (dd,  $J=13.2, 6.4$  Hz, H-Glc-6''), 3.72 (d,  $J=13.2$  Hz, H-Glc-6''), 3.82 (s, 3-OCH<sub>3</sub>) [18].

#### Verminoside (4)

The characteristics of verminoside (4) are as follows: yellow solid; m.p. 129.0–130.0 °C;  $[\alpha]_D^{25}$  -180.0° ( $c$  0.7, CH<sub>3</sub>OH); HRESIMS (negative)  $m/z$  523.1436 [M-H]<sup>-</sup>, calcd for C<sub>24</sub>H<sub>27</sub>O<sub>13</sub> 523.1452. <sup>1</sup>H-NMR (400 MHz, DMSO-*d*<sub>6</sub>)  $\delta_H$  5.08 (d,  $J=9.2$  Hz, H-1), 6.42 (d,  $J=6.0$  Hz, H-3), 4.93 (d,  $J=5.2, 8.8$  Hz, H-4), 2.47 (br s, H-5), 4.99 (d,  $J=6.8$  Hz, H-6), 3.64 (br s, H-7), 2.43 (br d,  $J=7.6$  Hz, H-9), 3.71 (br d,  $J=12.8$  Hz, H-10), 3.91 (br d,  $J=13.2$  Hz, H-10), 7.09 (d,  $J=2.0$  Hz, H-2'), 6.78 (d,  $J=8.4$  Hz, H-5'), 7.04 (dd,  $J=2.4, 8.4$  Hz, H-6'), 7.54 (d,  $J=15.6$  Hz, H-7'), 6.34 (d,  $J=15.6$  Hz, H-8'), 4.61 (d,  $J=7.6$  Hz, H-Glc-1''),

3.04 (m, H-Glc-2''), 3.19 (m, H-Glc-3''), 3.04 (m, H-Glc-4''), 3.15 (m, H-Glc-5''), 3.42 (dd,  $J=7.6, 12.0$  Hz, H-Glc-6'') 3.71 (br d,  $J=12.8$  Hz, H-Glc-6'') [19].

#### Isovanillyl catalpol (5)

The characteristics of isovanillyl catalpol (5) are as follows: light brownish powder; m.p. 145–150 °C;  $[\alpha]_D^{20}$  -98.1° ( $c$  0.199, CH<sub>3</sub>OH:CHCl<sub>3</sub> 1:1); HRESIMS (negative)  $m/z$  511.1478 [M-H]<sup>-</sup>, calcd for C<sub>22</sub>H<sub>27</sub>O<sub>13</sub> 511.1452. <sup>1</sup>H-NMR (400 MHz, DMSO-*d*<sub>6</sub>)  $\delta_H$  5.10 (d,  $J=9.2$  Hz, H-1), 6.42 (dd,  $J=6.0$  Hz, 1.6, H-3), 4.95 (dd,  $J=6.0, 4.0$  Hz, H-4), 2.50 (m, H-5), 5.05 (dd,  $J=8.4, 1.2$  Hz, H-6), 3.72 (d,  $J=8.4$  Hz, H-7), 2.47 (d,  $J=9.2$  Hz, H-9), 3.72 (d,  $J=13.2$  Hz, H-10), 3.92 (d,  $J=13.2$  Hz, H-10), 7.41 (d,  $J=2.0$  Hz, H-2'), 7.04 (d,  $J=8.4$  Hz, H-5'), 7.48 (dd,  $J=8.4$  Hz, 2.0, H-6'), 4.63 (d,  $J=7.6$  Hz, H-Glc-1''), 3.05 (d,  $J=7.6$  Hz, H-Glc-2''), 3.17 (m, H-Glc-3''), 3.02 (d,  $J=8.0$  Hz, H-Glc-4''), 3.14 (m, H-Glc-5''), 3.43 (dd,  $J=13.2$  Hz, 6.8, H-Glc-6''), 3.72 (dd,  $J=13.2$  Hz, 6.0, H-Glc-6''), 3.84 (s, 4-OCH<sub>3</sub>) [20].

#### 6-O-Veratroyl catalpol (6)

The characteristics of 6-O-veratroyl catalpol (6) are as follows: crystalline needles; m.p. 216–218 °C;  $[\alpha]_D^{20}$  -163.7° ( $c$  0.1, CH<sub>3</sub>OH); HRESIMS (negative)  $m/z$  525.1580 [M-H]<sup>-</sup>, calcd for C<sub>24</sub>H<sub>29</sub>O<sub>13</sub> 525.1608. <sup>1</sup>H-NMR (400 MHz, DMSO-*d*<sub>6</sub>)  $\delta_H$  5.11 (d,  $J=9.02$  Hz, H-1), 6.43 (dd,  $J=2.0, 6.0$  Hz, H-3), 4.97 (d, H-4), 2.59 (m, H-5), 5.09 (d,  $J=8.8$  Hz, H-6), 3.71 (br s, H-7), 2.47 (m, H-9), 3.71 (d, H-10), 3.92 (d,  $J=13.2$  Hz, H-10), 7.47 (d,  $J=2.4$  Hz, H-2') 7.10 (d,  $J=8.8$  Hz, H-5'), 7.45 (dd,  $J=2.0, 8.4$  Hz, H-6'), 4.62 (d,  $J=7.6$  Hz, H-Glc-1''), 3.06 (d,  $J=8.0, 7.6$  Hz, H-Glc-2''), 3.17 (m, H-Glc-3''), 3.02 (m, H-Glc-4''), 3.14 (m, H-Glc-5''), 3.43 (dd,  $J=13.2, 6.4$  Hz, H-Glc-6''), 3.72 (d,  $J=13.2$  Hz, H-Glc-6'') [20].

#### Preparation of sample, quantification and validation

##### UPLC-QTOF-MS profiling conditions

The compounds from the *P. rotundum* extract (1 mg/mL, 2  $\mu$ L) were analyzed using UPLC-PDA-QTOF-MS. The gradient included A and B mobile phase solutions (A: water with 0.1% FA; B: can with 0.1% FA) as follows: 0.0–1.0 min, 12% B; 1.0–9.0 min, 12–13% B; 9.0–10.0 min, 13–14% B; 10.0–13.0 min, 14% B; 13.0–15.0 min, 14–18% B; 15.0–16.5 min, 18–22% B; 16.5–20.0 min, 22–14% B; 20.0–20.1 min, 22–100% B; and 20.1–22.5 min, 100% B. MS was performed in negative ion mode ([M-H]<sup>-</sup>). N<sub>2</sub> was used as the desolvation gas, and the desolvation temperature was set to 350 °C at flow rates of 800 L/h and 50 L/h with a source temperature of 110 °C. The capillary and cone voltages were set to 2.3 kV and 40 V, respectively. The data for each sample were collected with a scan time of 0.25 s and a 0.01 s interscan delay. Leucine



enkephalin was used as the reference compound ( $m/z$  554.2615,  $ESI^-$ ). The analysis was performed on a UPLC T3 column (Waters Corporation, Milford, MA). Exact MS, MS/MS, and elemental analysis were confirmed using UNIFI (v1.9, Waters) software incorporated into the Waters instrument.

#### **Limit of detection, limit of quantification, analytical curve and linearity, recovery, selectivity and matrix effect**

LC analysis of the extract was performed to determine whether the six compounds selected as marker components were included in the 70% EtOH extract. The calibration curves and quantification were analyzed under the same conditions as those used for MS profiling. The peak areas of major marker components 1–6 at different growth periods were integrated from the chromatogram at 254 nm using processing instrument control software. Peak areas integrated into linear models of standard calibration curves of six components were calculated, and the content of each compound was calculated and comparatively analyzed to determine the optimal harvest time for *P. rotundum*. Standard stock solutions (1 mg/mL) of six iridoids were prepared in EtOH, and the calibration curve was plotted using linear regression by 6-point dilution with a concentration range of 0.5–500  $\mu\text{g/mL}$ . LODs were set using an equation of  $3.3\sigma/S$ , and the LOQs were set using an equation of  $10\sigma/S$ . It was reviewed according to the ICH guidelines for pharmaceuticals (ICH, 2005). To determine the accuracy of the developed assay, interday and intraday variability was checked with 3 different concentrations and 6 replicate assays over 3 consecutive days. Precision was determined by the RSD as a change in peak area, and accuracy was assessed by standard recovery from the extract. Six repetitions were performed to evaluate all experiments, and the average recovery was determined [Recovery (%) = (measured/original)  $\times$  100%]. Acceptable recoveries ranging from 70 to 120% and RSD below 20% were set considering recommended values.

#### **Total polyphenol and total flavonoid contents**

The total phenol content (TPC) of *P. rotundum* was determined according to the Folin–Denis reagent method [21]. In this assay, 10  $\mu\text{L}$  of samples, 10  $\mu\text{L}$  of 2%  $\text{Na}_2\text{CO}_3$ , and 10  $\mu\text{L}$  of 50% reagent were mixed, the absorbance was measured at 725 nm, and the gallic acid equivalent was quantified using a standard curve. The total flavonoid content (TFC) of *P. rotundum* samples was determined [21]. Then, 0.5 mL of extract was mixed with 0.1 mL of 10%  $\text{Al}(\text{NO}_3)_3$  and 0.1 mL of 1 M  $\text{CH}_3\text{CO}_2\text{K}$ , the absorbance was measured at 420 nm, and quercetin equivalents were quantified using a standard curve.

#### **Measurement of antioxidant activity**

The antioxidant inhibition assays of DPPH and ABTS were run in 0.15 mM DPPH in EtOH and a 7 mM ABTS stock solution with 2.45 mM potassium persulfate mixed 1:1 (v/v), respectively [22]. The amount of DPPH and ABTS radicals remaining was measured with and without the extract solution at 517 nm after 30 min and 734 nm ( $E = [(A_c - A_t)/A_c] \times 100$ ).

#### **NCI-H292 cell culture and MUC5AC ELISA**

NCI-H292 airway epithelial cells were purchased from the American Type Culture Collection (CRL-1848; ATCC, Manassas, VA, USA). The cells were grown in complete medium composed of RPMI 1640 medium, 10% FBS and 100 units/mL penicillin combined with 100  $\mu\text{g/mL}$  streptomycin. The cells were incubated in a humidified incubator at 37 °C and in a 5%  $\text{CO}_2$  atmosphere. Cells ( $5 \times 10^4$  cells/mL) were seeded in 96-well plates 1 day prior with complete medium. The cells were pretreated with the indicated concentrations of test samples for 2 h and then stimulated with 25 nM PMA for 16 h. Secreted MUC5AC protein in culture supernatants was analyzed by ELISA as described previously [23]. Mouse monoclonal MUC5AC antibody (Abcam, Cambridge, UK; 1:500 in blocking buffer) was used for the primary reaction. Finally, the absorbance was measured at 450 nm using an Epoch microplate reader (BioTek instruments, Inc., Winooski, VT).

#### **Statistical analysis**

All measurements were made in triplicate. The results were analyzed and presented using SigmaPlot 2001 (Systat Software Inc., Chicago, IL, USA).

## **Results and discussion**

#### **Single-factor extraction optimization**

To prepare a standardized extract for raw material development, the contribution of ethanol concentration, extraction time, and extraction temperature to iridoid content was accomplished by keeping two of the three extraction factors constant and changing the other to determine the optimal extraction conditions. This experiment was performed on verproside, which had the highest content among the extracts. From Additional file 1: Fig S1, the major metabolite tended to increase with increasing ethanol concentration over a 2 h extraction period at room temperature with 10, 30, 50, 70 and 95% EtOH concentrations; the concentration of 70% EtOH achieved the highest area. The verproside area response to increasing water bath temperature during the 2 h extraction period in 70% ethanol followed a similar trend to that observed in previous EtOH factor experiments

and peaked at 40 °C. The optimal extraction time for all three evaluation indicators was 1 h since there was little difference in the verproside area. Therefore, we selected 70% ethanol at 40 °C for 1 h for the extraction of six major markers from the aerial parts of *P. rotundum*.

#### Multivariate statistical analysis of *P. rotundum* at different growth stages

We determined the difference in the metabolites of various growth stages (harvested time: July 15 & 29, and August 12 & 26) from the optimally prepared extracts of the aerial parts using UPLC-Q-TOF-MS. To visualize clustering patterns, PCA and OPLS-DA were used. PCA, which is an unsupervised analysis, diminishes the multidimensionalities of complex data sets to lower-level dimensions and provides an overview of observations such as groupings, patterns, and outliers [24]. It is an effective approach to visualize clustering patterns to discover ultimate differences. In the PCA, the score plot of each sample is shown in Fig. 1A. In the PCA score plot, the mid and late July and mid and late August groups were clearly divided. Additionally, each group was clearly divided by week.

OPLS-DA was analyzed to identify major markers with a high contribution to clustering between July and August. In the OPLS-DA score plot, the data were clearly separated, and the scores  $t[1]$  and  $to[1]$  were significant variables between the July and August groups (Fig. 1B). An S-plot was applied to select the decisive variables that presented the covariance  $w[1]$  and correlation  $p$  (corr) [1] among them. The OPLS-DA model identified metabolites that ultimately showed differences between July and August. Metabolites in the right region of the S-plot showed elevated components in August, and metabolites in the left region showed increased metabolite markers in July. Metabolites had a higher contribution and confidence to the variance between the two groups since the points were located further along the x- and y-axes. Various metabolites identified in the S-plot were confirmed as potential marker candidates for differences in growth periods (Fig. 1C). Although these biomarkers were present in both July and August, they were more numerous in August than in July and were identified as specific biomarkers in August.

#### Metabolite analysis by using MS and NMR

The ethanol sample of *P. rotundum* was analyzed by UPLC-ESI-QTOF-MS. *P. rotundum* belongs to the family Scrophulariaceae and is rich in iridoid glycosides [25]. More sensitive MS detection of iridoid glycosides occurred in negative ionization mode than in positive ionization mode [Ref.] Therefore, we identified all isolated compounds (1–6 in negative mode), and all data

were detected from the deprotonated molecule  $[M-H]^-$  in the MS/MS spectra (Fig. 2, Additional file 1: Fig. S2, S3). The UV spectrum showed absorption peaks at 220, 263 and 296 nm, indicating the presence of a conjugated enol–ether system. High-resolution electrospray ionization mass spectrometry (HRESIMS) analysis of the molecular ion cluster  $[M-H]^-$  ( $m/z$  497.1317) of verproside (1), as the major compound in *P. rotundum*, established the molecular formula as  $C_{20}H_{20}O_5$ . The MS fragment detected at  $m/z$  335.0778  $[M-H-162]^-$  corresponded to the loss of the glucose moiety; the loss of 114 Da (fragment ion at  $m/z$  221.0443  $[M-H-162-114]^-$ ) was due to the loss of two aldehyde groups and cleavage of the substituent ring (28 Da), which was based on the hemiacetal group being easily converted into an epimeric isomer. Therefore, the hemiacetal group isomerized into two aldehyde groups. For these reasons, compound 1 was identified as verproside. Compounds 2–6 exhibited  $[M-H]^-$  ions at  $m/z$  as follows: 481.1370 (2; calcd for  $C_{22}H_{26}O_{13}$ , 481.1352,  $t_R = 8.98$  min), 523.1475 (3; calcd for  $C_{24}H_{28}O_{13}$ , 523.1457,  $t_R = 11.54$  min), 511.1473 (4; calcd for  $C_{23}H_{28}O_{13}$ , 511.1457,  $t_R = 11.06$  min), 511.1473 (5; calcd for  $C_{23}H_{28}O_{13}$ , 511.1457,  $t_R = 12.48$  min), and 525.1630 (6; calcd for  $C_{24}H_{30}O_{13}$ , 525.1614,  $t_R = 17.54$  min). These compounds also showed fragment ion losses similar to those of verproside (1): glucose (–162 Da) and two aldehyde groups and cleavage of the substituent ring of the iridoid backbone ( ${}^6,9X^-$  ion, –114 Da). Therefore, these compounds were tentatively identified as catalposide (2), verminoside (3), picroside II (4), isovanillyl catapol (5), and 6-*O*-veratroyl catalpol (6) [17–20, 26].

Six compounds (1–6) were obtained from the aerial parts of *P. rotundum*, and their structure elucidation was confirmed based on reported NMR literature information. The discussion for structural elucidation will focus on compound 1, which has been identified as the main metabolite. Compound 1 was deduced to be a glucoside according to the general appearance of its  ${}^1H$  and  ${}^{13}C$  NMR spectra (Additional file 1: Fig S1–S12). The  ${}^{13}C$  NMR data showed 22 carbons, including five quaternary carbons, two methylene carbons and fifteen methine carbons. The  ${}^1H$  and  ${}^{13}C$  NMR spectra suggested an iridoid-type skeleton with one glucoside unit [ ${}^{13}C$  NMR:  $\delta_C$  98.3 (C-Glc-1''), 73.9 (C-Glc-2''), 76.9 (C-Glc-3''), 70.7 (C-Glc-4''), 77.9 (C-Glc-5''), 61.8 (C-Glc-6'');  ${}^1H$  NMR:  $\delta_H$  4.61 (d,  $J=7.8$  Hz, H-Glc-1''), 3.06 (d,  $J=7.8$  Hz, H-Glc-2''), 3.17 (m, H-Glc-3''), 3.02 (d,  $J=8.8$  Hz, H-Glc-4''), 3.14 (m, H-Glc-5''), 3.47 (dd,  $J=6.8, 11.6$  Hz, H-Glc-6'' a), 3.72, (m, H-Glc-6'' b)]. The  ${}^1H$  NMR signals from the aglycone moiety showed five aromatic/olefinic methines [ $\delta_H$  7.40 (d,  $J=2.0$  Hz, H-2'), 7.36 (dd,  $J=2.0, 8.4$  Hz, H-6'), 6.83 (d,  $J=8.4$  Hz,

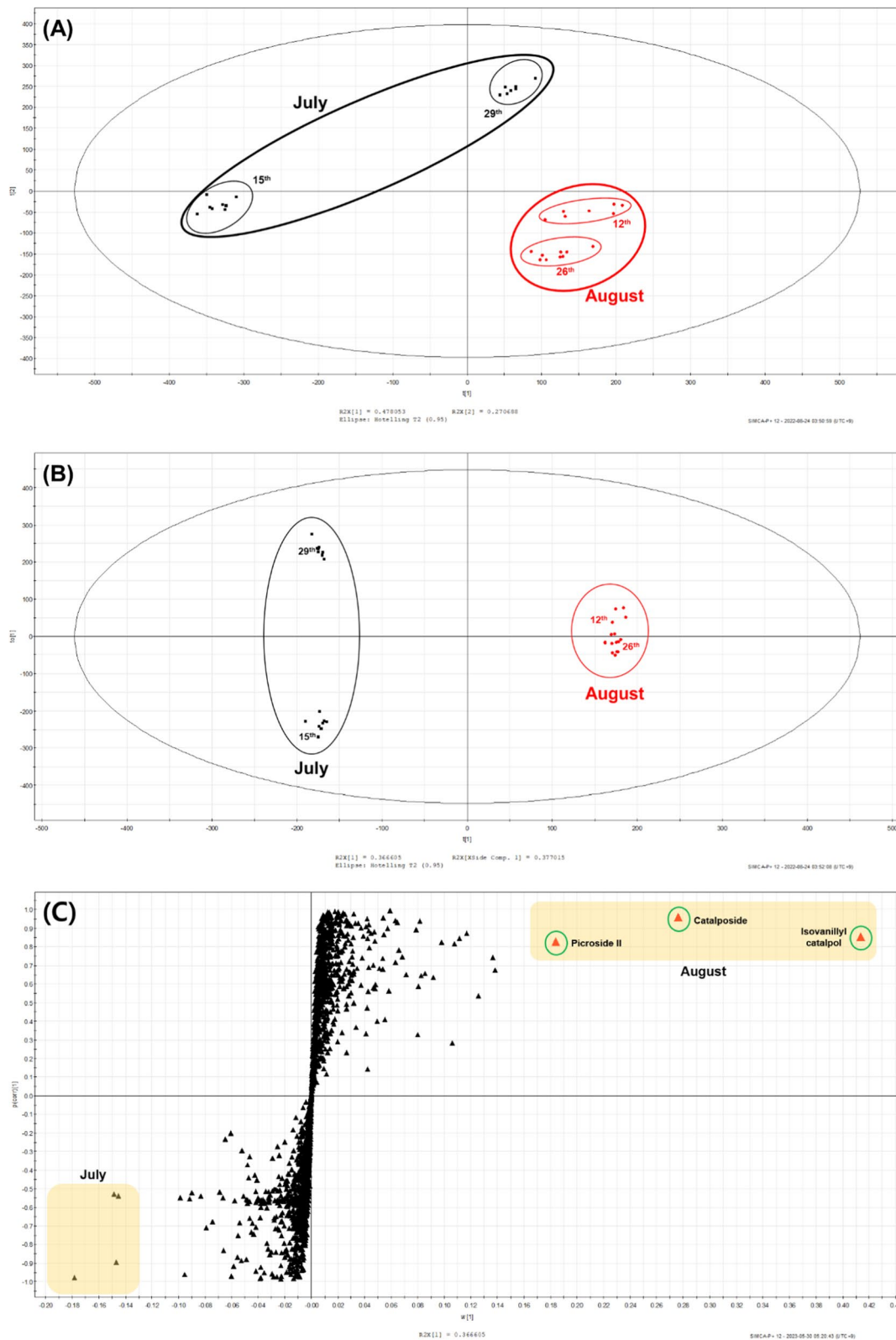


**Fig. 1** A Principle component analysis (PCA) score plot, B Orthogonal Partial Least Squares Discriminant Analysis (OPLS-DA) score plot and C S-plot in *P. rotundum* var. *subintegrum* at different growth stages.

H-5'), 6.42 (dd,  $J=1.6, 5.6$  Hz, H-3), 4.94 (dd,  $J=4.4, 5.6$  Hz, H-4)], three oxygenated methines [ $\delta_{\text{H}}$  5.10 (d,  $J=9.2$  Hz, H-1), 5.04 (dd,  $J=0.8, 8.0$  Hz, H-6), 3.69 (d,  $J=8.0$  Hz, H-7)], an oxymethylene [ $\delta_{\text{H}}$  3.92 (d,  $J=13.6$  Hz, H-10a), 3.72 (d,  $J=13.6$  Hz, H-10b)], and two methines [ $\delta_{\text{H}}$  2.50 (m, H-5), 2.47 (d,  $J=8.0$  Hz, H-9)]. The  $^{13}\text{C}$  NMR spectrum showed 16 carbon resonances, including a carbonyl carbon [ $\delta_{\text{C}}$  166.1 (C-7')], three oxygenated aromatic/olefinic quaternary carbons [ $\delta_{\text{C}}$  151.3 (C-4'), 145.6 (C-3'), 120.4 (C-1')], an oxygenated quaternary carbon [ $\delta_{\text{C}}$  66.2 (C-8)], five aromatic/olefinic methanes [ $\delta_{\text{C}}$  141.6 (C-3), 122.6 (C-5'), 116.8 (C-2'), 115.8 (C-6'), 102.2 (C-4)], three oxygenated methines [ $\delta_{\text{C}}$  93.4 (C-1), 79.9 (C-6), 58.9 (C-7)], an oxymethylene [ $\delta_{\text{C}}$  58.7 (C-10)], and two methines [ $\delta_{\text{C}}$  42.3 (C-9), 35.7 (C-5)]. The HMBC correlations from H-2' to C-4'/C-6'/C-7', H-5' to C-1'/C-3', and H-6' to C-2'/C-4'/C-7' showed the presence of a dihydroxybenzoyl group, and the HMBC correlation from H-6 to C-7' suggested that the dihydroxybenzoyl group was attached to C-6 in the structure of 1. The glucose moiety was identified as being linked at C-1 based on the HMBC correlation from H-1 to C-Glc-1". Therefore, the structure of compound 1 was deduced as shown in Fig. 2A and identified as verproside. The NMR data

of the other isolated compounds (2–6) were quite similar to those of verproside (1), except for the oxygen bridge between C-7 and C-8 and the substituent groups at C-6. Compounds 2–6 differed by only their replacement of the 3-methoxy-4-hydroxybenzoyl group at C-6 with 4-hydroxybenzoyl, 3,4-dihydroxyphenyl, 3-hydroxy-4-methoxybenzoyl, and 3,4-dimethoxybenzoyl groups, respectively. Thus, compounds 2–6 were identified as catalposide (2), verminoside (3), picroside II (4), isovanillyl catapol (5), and 6-*O*-veratroyl catalpol (6), and the structures of these compounds are shown in Fig. 2A.

#### Analytical method validation

For iridoid profiling analysis of the aerial parts of *P. rotundum*, the UPLC-ESI-QTOF-MS method was applied, and the experimental method described in Sect. 2.6.2 was performed for major marker components 1–6. All curves confirmed linearity in the test range  $r^2 \geq 0.998$ , and the LODs/LOQs of the six components were identified to be 0.12–0.28  $\mu\text{g/mL}$  and 0.32–0.97  $\mu\text{g/mL}$ , respectively (Additional file 1: Table S3). The RSD values for six analytes were less than 2% (Table 1). Aerial parts of *P. rotundum* were

**Table 1** The results of precision (intra, inter-day) and accuracy (recovery) of isolated iridoids 1–6

Iridoids	Content (mg/g)	Sample mg/mL	Intra-day (n=6)		Inter-day (n=18)		Accuracy (n=6)				
			SD	RSD (%)	SD	RSD (%)	Spiked (mg/g)	Theoretical amount ( $\mu\text{g/mL}$ )	Recorded amount ( $\mu\text{g/mL}$ )	Recovery (%)	RSD (%)
1	85.446	1.0	8.20	1.98	1.52	1.63	50.0	135.45	138.02	101.97	0.63
		2.0	16.64	1.95	–	–	100.0	185.45	187.12	100.95	0.89
		4.0	9.72	1.18	–	–	200.0	285.45	288.25	100.98	0.50
2	9.361	1.0	1.59	1.75	0.19	1.93	12.5	21.86	22.04	100.82	1.03
		2.0	3.66	2.00	–	–	25.0	34.36	34.45	100.27	1.24
		4.0	6.05	1.64	–	–	50.0	59.36	59.16	99.67	1.11
3	11.664	1.0	2.16	1.91	0.26	1.98	12.5	24.16	24.27	100.45	0.77
		2.0	2.63	1.11	–	–	25.0	36.66	36.79	100.33	1.16
		4.0	9.12	1.93	–	–	50.0	61.66	60.90	98.77	1.77
4	9.149	1.0	1.60	1.90	0.19	1.85	12.5	21.65	21.69	100.20	0.68
		2.0	3.17	1.80	–	–	25.0	34.15	34.18	100.08	0.80
		4.0	3.69	1.05	–	–	50.0	59.15	56.18	94.97	1.59
5	24.186	1.0	4.61	1.96	0.21	0.87	25.0	49.19	49.14	99.93	0.80
		2.0	8.60	1.77	–	–	50.0	74.19	73.37	98.91	0.61
		4.0	15.72	1.68	–	–	100.0	124.19	126.10	101.54	1.18
6	12.934	1.0	2.43	1.90	0.17	1.31	12.5	25.43	25.05	98.58	1.16
		2.0	5.64	1.97	–	–	25.0	37.93	37.31	98.42	0.95
		4.0	10.51	1.92	–	–	50.0	66.72	67.16	100.65	0.87



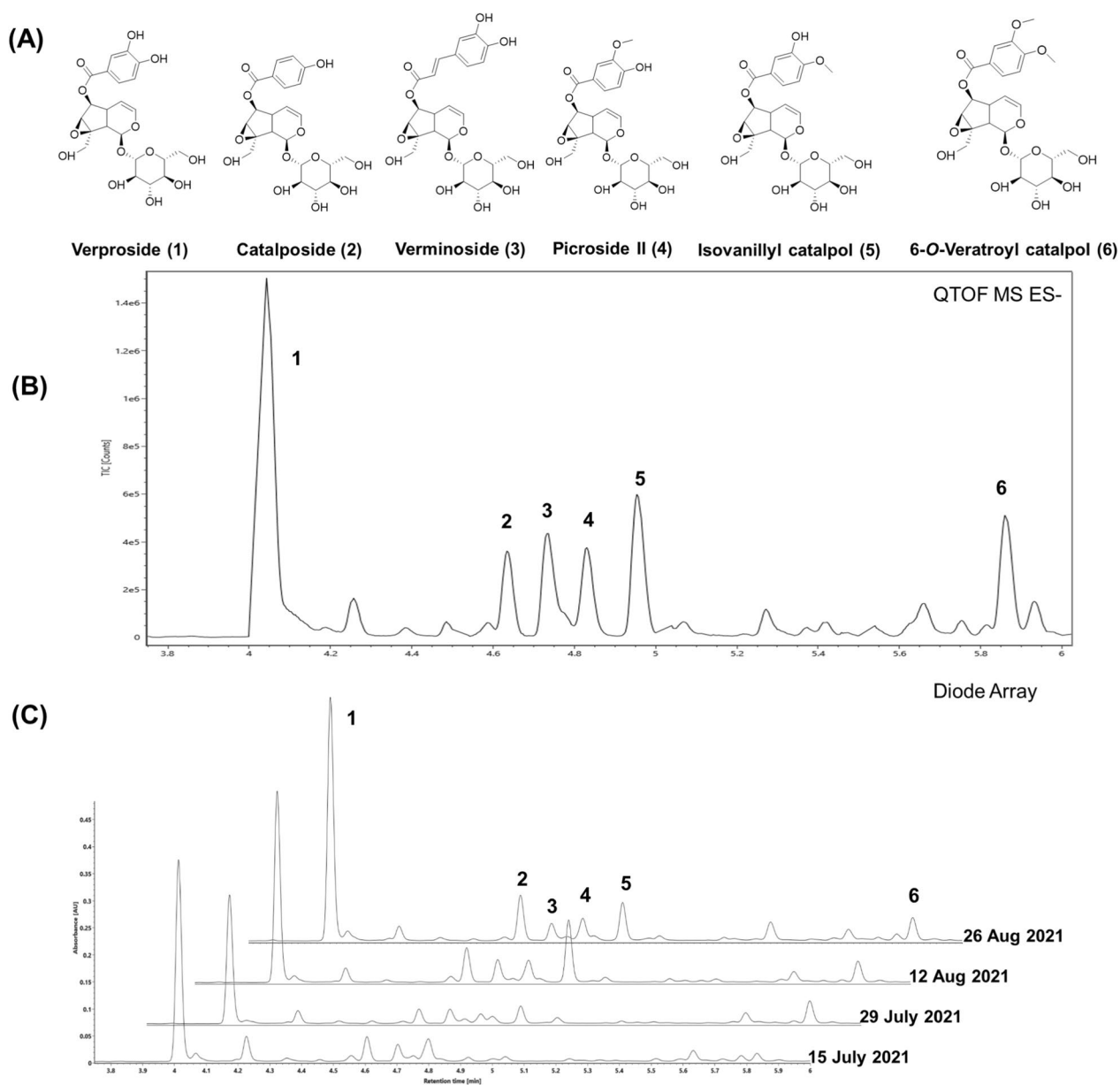


**Fig. 2** **A** Chemical structures of isolated compounds 1–6 from the aerial parts of *P. rotundum* var. *subintegrum*. **B** Representative UPLC-QTOF-MS chromatogram of August extract. **C** UPLC profiles of *P. rotundum* var. *subintegrum* extracts from the four different sampling dates (July–August) examined.

prepared in EtOH, and six components were added to evaluate accuracy with recovery tests of the six components from spiked samples at three concentrations. The RSD of the six components was less than 2%, confirming the recovery rate of 94.97–101.97% (Table 1). Validation analysis results confirmed that the method established by UPLC was accurate and quantified major marker components 1–6 in the aerial part extract of *P. rotundum*.

#### Iridoid contents of *P. rotundum* at different growth periods

The crop growth stage was divided into the sprout (stage 1), seedling (stage 2), vegetative (stage 3), budding (stage 4), flowering (stage 5), and ripening stages (stage 6). Five weeks after seeding, the aerial parts of *P. rotundum* were collected in three separate plots per week from 5 to 11 weeks (stage 2–6) to investigate whether the contents of verproside (1), catalposide (2), verminoside (3), picoside II (4), isovanillyl catapol (5), and 6-O-veratroyl catalpol

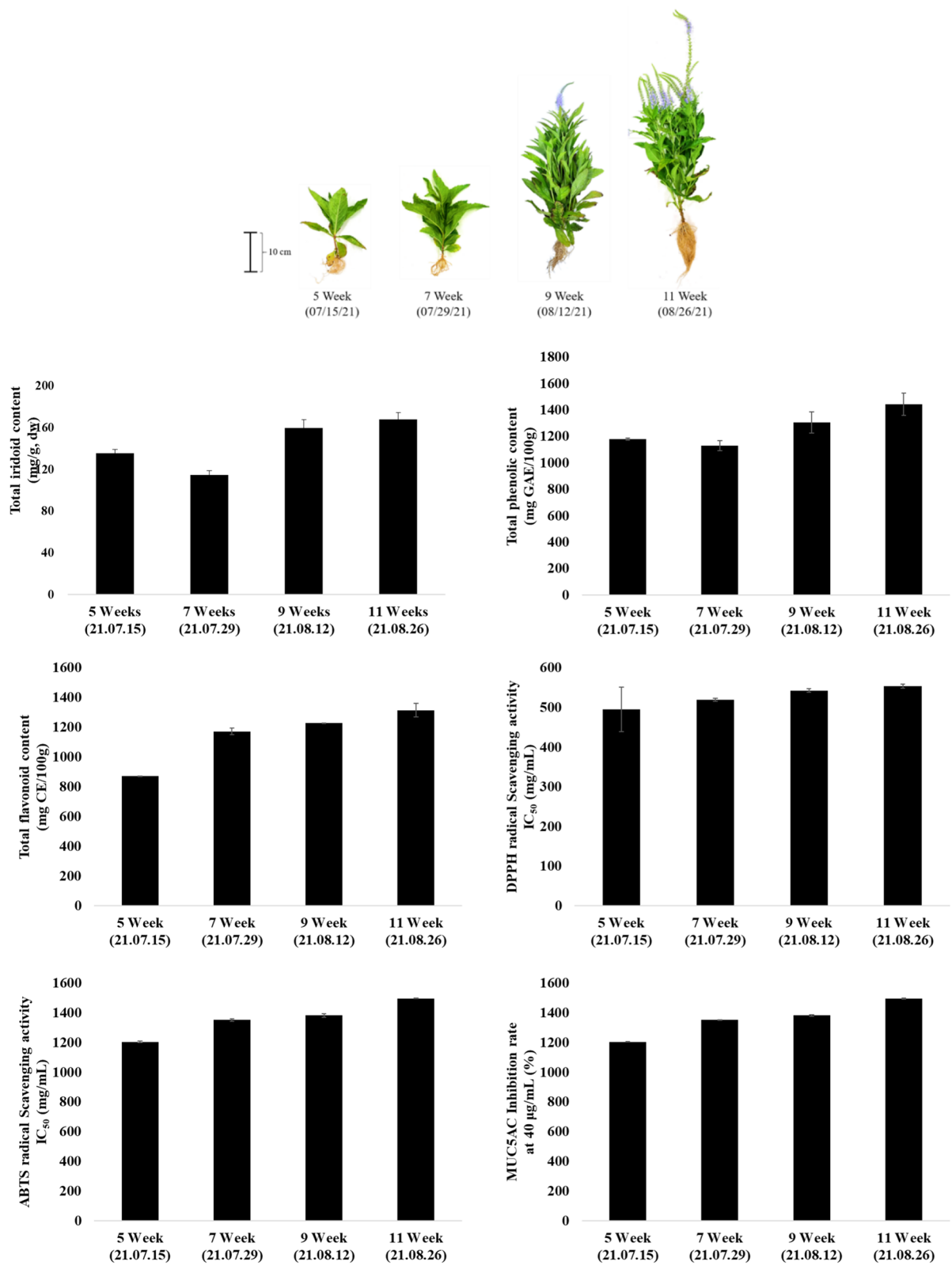


**Fig. 3** Total iridoid, totalphenolic, flavonoid contents, DPPH, ABTS, and MUC5AC inhibition in extracts of *P. rotundum* var *subintegrum* at growth stages.

(6) were changed by the growth period of *P. rotundum* (Fig. 2C). The aerial parts of these plants were grown and collected for 2 months at different growth periods of approximately 18.5–34.3 cm and 1.67–10.84 g (Additional file 1: Table S2). As shown in Fig. 3, the yield of plant materials increased according to the growth period, and the content of major marker components 1–6 tended to increase rapidly in August (July 114.56–135.6 and August 159.87–167.69 mg/g, respectively) when there was a high amount of precipitation and a low duration of sunshine (Additional file 1: Table S2). Sample preparation, quantification and validation of six components contained in the aerial parts of *P. rotundum* collected by growing period were quantified by analytical methods according to Sect. 2.6. As shown in Table 2, the concentrations of verproside (1), catalposide (2), picroside II (4), and isovanillyl catapol (5) increased rapidly over time from August (1: 82.18 mg/g in July, 98.57 mg/g in August; 2: 5.97 mg/g in July, 10.99 mg/g in August; 4: 6.42 mg/g in July, 9.11 mg/g in August; 5: 4.42 mg/g in July, 20.00 mg/g in August); however, the concentrations of verminoside (3) and 6-*O*-veratroyl catalpol (6) tended to slightly decrease on an average monthly with the growth of the aerial parts of *P. rotundum* (3: 11.94 mg/g in July, 11.58 mg/g in August; 6: 14.13 mg/g in July, 13.77 mg/g in August). In particular, the two main markers 2 and 5 of the aerial parts showed a high correlation after a large amount of precipitation and low duration of sunshine in August by microclimate factors. Therefore, it was found that precipitation and sunshine hours were the main factors for the six components of aerial parts of *P. rotundum*, but it seems that the factors of temperature, wind, and relative humidity could not be perfectly excluded. Therefore, a microclimate in August cannot be ruled out and is expected to have an effect on promoting the biosynthetic pathway from verproside (1) to catalposide (2) and isovanillyl catapol (5)

through *O*-methylation. Although the biosynthetic pathways of the iridoids presented in this study could not be represented as all biosynthetic pathways, catalposide and isovanillyl catapol were shown to be derivatized from verproside. This result of the possible metabolic pathways of the two highly dependent metabolites and the correlation analysis of iridoids confirmed the correlation between verproside and two metabolites in a previous study [27]. Moreover, iridoids with increased content may in some cases be related to plant defense mechanisms, and their biological role in plants may be related to self-protection against insects and herbivores [28]. Iridoid glycosides are normally activated by β-glucosidases in the intestines of insect herbivores, which act as a deterrent to unadapted insects, giving them adaptability to plants containing iridoid glycosides [29, 30]. Therefore, a limited discussion from different harvest periods of *P. rotundum* was provided because iridoid metabolites are key constituents in plants.

**Correlation between the iridoid metabolites and biological activities of *P. rotundum* at different growth stages**

In vitro screening, including TPC, TFC, DPPH and ABTS, is simple, reproducible, and stable, making it one of the most attractive targets for screening experiments in natural products (crops, beverages, foods, fruits and vegetables) because of the easy access to antioxidants [31–35].

Excessive secretion of mucus in patients with respiratory diseases not only interferes with normal breathing but also reduces the primary immune response [36]. Given that mucin secretion is partly associated with the inflammatory response of epithelial cells, antioxidant pharmacological approaches to modulate mucin production or secretion are valuable. MUC5AC, a component of mucin, is recognized as a target protein for disease treatment because of its adhesive and viscoelastic nature.

**Table 2** Isolated iridoids 1 – 6 contents of *P. rotundum* var. *subintegrum*

Harvest date	Growth weeks	Iridoids content (mg/g, dw)*					
		1	2	3	4	5	6
15 Jul 2021	5th	96.97 ± 2.44	7.13 ± 0.12	12.27 ± 0.34	8.62 ± 0.53	0.81 ± 0.04	9.79 ± 0.20
29 Jul 2021	7th	67.39 ± 2.59	4.82 ± 0.15	11.61 ± 0.27	4.22 ± 0.21	8.04 ± 0.25	18.47 ± 0.79
Average		82.18	5.97	11.94	6.42	4.42	14.13
12 Aug 2021	9th	88.09 ± 3.91	9.53 ± 0.25	14.63 ± 0.85	9.36 ± 0.42	24.96 ± 1.16	13.30 ± 1.19
26 Aug 2021	11th	109.05 ± 4.25	12.45 ± 0.44	8.53 ± 0.36	8.38 ± 0.30	15.05 ± 0.64	14.24 ± 0.82
Average		98.57	10.99	11.58	9.11	20.00	13.77

Comp. 1, verproside; Comp. 2, catalposide; Comp. 3, verminoside; Comp. 4, picroside II; Comp. 5, isovanillyl catapol; Comp. 6, 6-*O*-veratroyl catalpol.

Samples harvested once every two weeks were determined by UPLC-PDA at UV 254 nm, and each sample was injected in sextuplicate

\*The mean ± standard deviation of sextuplicate experiments

**Table 3** Total phenolic, flavonoid contents, DPPH, ABTS, and MUC5AC inhibition in extracts of *P. rotundum* var *subintegrum* at growth stages

<i>P. rotundum</i>	Total phenolic content (mg GAE/100 g) <sup>a</sup>	Total flavonoid content (mg CE/100 g) <sup>b</sup>	DPPH radical Scavenging activity IC <sub>50</sub> (mg/mL) <sup>c</sup>	ABTS radical Scavenging activity IC <sub>50</sub> (mg/mL) <sup>c</sup>	MUC5AC Inhibition rate at 40 µg/mL (%) <sup>d</sup>
15 Jul 2021	1178.1 ± 6.2	870.4 ± 1.7	0.49 ± 0.05	1.20 ± 0.04	48.6 ± 0.9
29 Jul 2021	1129.7 ± 37.5	1171.1 ± 22.7	0.52 ± 0.03	1.35 ± 0.09	21.4 ± 1.0
Average	1153.9	1020.8	0.51	1.28	35.0
12 Aug 2021	1304.1 ± 81.7	1227.6 ± 0.7	0.54 ± 0.05	1.38 ± 0.01	17.7 ± 3.5
26 Aug 2021	1442.5 ± 84.4	1313.2 ± 45.8	0.55 ± 0.05	1.49 ± 0.01	50.0 ± 4.7
Average	1373.3	1270.4	0.55	1.44	33.9

<sup>a</sup> Gallic acid equivalent (GAE) was used as a standard for measuring the total phenolic content

<sup>b</sup> Catechin equivalent (CE) was used as a standard for measuring the total flavonoid content

<sup>c</sup> Effective activity was expressed as the mean of 50% IC (half maximal inhibitory concentration) of triplicate experiments

<sup>d</sup> Data presented are the inhibition rate mean ± S.D. of triplicate experiments

Several researchers have reported antioxidant and MUC5AC inhibitory activities of plant extracts under fermentation and germination methods [37]. Therefore, we aimed to correlate iridoid contents with potency in different growth periods (5–11 weeks) to examine the evidence for industrial sources as functional crops. Significant differences in TPC and TFC were observed among the four samples, as shown in Fig. 3; Table 3. According to their results, samples collected during the growth period gradually showed differences in content and potency. TPC and TFC in July were observed at 1153.9 GAE mg/g and 1020.8 CE mg/g; the August samples exhibited high TPC and TFC in the following order: 1373.3 GAE mg/g and 1270.4 CE mg/g greater than those in July. In the DPPH and ABTS results, the harvested *P. rotundum* extract was similar to the present data in that the TPC and TFC results correlated as the radical scavenger activity was related to phenolic and flavonoid metabolites. The highest average DPPH and ABTS scavenging capacities were observed in samples on Aug. 26 of the aerial parts with 0.49 and 120 mg/mL, respectively, followed by Aug. 12 (0.52 and 1.35 mg/mL) > Jul. 29 (0.54 and 1.38 mg/mL) > Jul. 15 (0.55 and 1.49 mg/ml). Notably, the scavenging activities for DPPH radicals in all collected samples were higher than those for ABTS radicals, similar to the data obtained in previous studies. Additionally, the findings of the current research indicated that the TPC, TFC, DPPH, and ABTS distributions could be confirmed by the release of hydroxyl moieties from phenolic structures (2, 4, and 5) in the harvested *P. rotundum* extract (Table 2). Additionally, the average antioxidant capacity during the growth period was as follows in decreasing order: Aug. 26 > Aug. 12 > Jul. 29 > Jul. 15. Our analyzed data can be compared with previous studies that *Cudrania tricuspidata* [14] and *Aloe vera* [38]

displayed high TPC, TFC, DPPH, and ABTS compared in different growth stages. The MUC5AC inhibition rate of the extracts by harvest time is listed in order of high: Aug. 26 > Jul. 15 > Jul. 29 > Aug. 12. Notably, the efficacy of inhibiting MUC5AC secretion by harvest time of each extract reflects changes in iridoid 1 and 2 contents of each extract. Consequently, iridoid contents in the aerial parts of *P. rotundum* were potentially responsible for the antioxidant effects against TPC, TFC, DPPH, ABTS and MUC5AC inhibition activities, which had been shown in previous studies. The aerial parts of *P. rotundum* can be evaluated through the evaluation of basic biological activity and respiratory target efficacy and be recommended as a source for use as a natural raw material for drug and health claims.

**Table 4** Comparison of contents of iridoids 1–6 in cultivated *P. rotundum* extract in August according to the contents of ATC1 reported in the literature

Iridoids	ATC1 extract (area %) <sup>a,b</sup>	August 40% extract (area %)	August 70% extract (area %)
Verproside 1	17.60	22.77	24.47
Catalposide 2	0.72	4.22	4.55
Verminoside 3	2.62	2.51	2.80
Picroside II 4	1.20	2.92	3.29
Isovanillyl catapol 5	1.26	1.25	1.35
6-O-veratroyl catalpol 6	2.36	2.46	2.53

<sup>a</sup> Calculated from patent KR 10-2014-0122656

<sup>b</sup> Dried the whole plant of *P. rotundum* (10 g) were extracted once in 40% ethanol (100 mL) and at room temperature for 48 h, and then second extracted at 80–100 °C reflux for 48 h. The extracts were combined and concentrated in vacuo at 40 °C to produce a dried extract (2.51 g), which was further extracted with *n*-BuOH (0.5ith *n*-BuOH (0.55 g), and H<sub>2</sub>O (1.9 g)

### Comparison of the August and ATC1 extracts for standardization

YPL-001 from the active fraction of *P. rotundum* showed good efficacy in reducing airway inflammation in human lung cell lines and in a mouse model of asthma and COPD. Therefore, the main six iridoids of YPL-001 were selected to constitute a drug candidate mixture that was named YPL-001, which has been developed as a natural drug. The relative contents of the main six iridoids contained in the aerial part of *P. rotundum* collected by growth period were quantified for comparison using the preparation method and analysis method described in a previous patent [39]. As shown in Table 4, verproside 1 showed the highest content of 17.60% in ATC1 as well as 22.77 and 24.47% in the 40% and 70% extracts from August, respectively. The iridoid 3–6 contents of ATC1 extracts were relatively stable in both the 40% and 70% extracts from August, and the contents of the extracts of the harvested raw materials were as follows: verminoside 3 (2.92–3.29%) > picroside II 4 (2.51–2.80%) > 6-O-veratroyl catalpol 6 (2.46–2.53) > isovanillyl catalpol 5 (1.25–1.35). Catalposide 2 had the highest content of 4.22–4.55% in the extract from August but had a relatively low content in ATC1 (0.72%). In summary, the study of secondary metabolites of existing natural resources and their extraction methods validates iridoid extraction and comparative content evaluation in our study. Current data provide important information on plant cultivation, harvest time, and distribution of major components.

### Supplementary Information

The online version contains supplementary material available at <https://doi.org/10.1186/s13765-023-00796-0>.

**Additional file 1: Table S1.** Soil chemical properties for growth and development of *P. rotundum* var. *subintegrum*. **Table S2.** Growth conditions and the features of *P. rotundum* var. *subintegrum*. **Table S3.** Coefficient of determination and limit of detection and quantification of 6 iridoids isolated from *P. rotundum* var. *subintegrum*. **Figure S1.** Single-factor extraction optimization. **Figure S2-1.** <sup>1</sup>H and <sup>13</sup>C NMR spectrum of Verproside (1). **Figure S2-2.** <sup>1</sup>H and <sup>13</sup>C NMR spectrum of Catalposide (2). **Figure S2-3.** <sup>1</sup>H and <sup>13</sup>C NMR spectrum of Verminoside (3). **Figure S2-4.** <sup>1</sup>H and <sup>13</sup>C NMR spectrum of Picroside II (4). **Figure S2-5.** <sup>1</sup>H and <sup>13</sup>C NMR spectrum of Isovanillyl catalpol (5). **Figure S2-6.** <sup>1</sup>H and <sup>13</sup>C NMR spectrum of 6-O-Veratroyl catalpol (6). **Figure S3-1.** UV, MS/MS and MS data of Verproside (1). **Figure S3-2.** UV, MS/MS and MS data of Catalposide (2). **Figure S3-3.** UV, MS/MS and MS data of Verminoside (3). **Figure S3-4.** UV, MS/MS and MS data of Picroside II (4). **Figure S3-5.** UV, MS/MS and MS data of Isovanillyl catalpol (5). **Figure S3-6.** UV, MS/MS and MS data of 6-O-Veratroyl catalpol (6).

### Acknowledgements

This work was supported by the KRIBB Research Initiative Program funded by the Ministry of Science and ICT (MSIT) of Republic of Korea. We thank the Korea Basic Science Institute, Ochang, Korea, for providing the NMR data.

### Author contributions

SSB, KDY, OSM, WSY, KIJ, LJH, and KSY performed the plant and soil sampling of the analysis samples and quantitative analysis; KMO, PJY, KNH, and KHY performed the biological analysis and helped with the preparation of the manuscript; HBY, RHW, and OSR collected and discussed the results; RHW designed and supervised all the results and wrote the manuscript. All authors read and approved the final manuscript.

### Funding

This work was supported by the KRIBB Research Initiative Program funded by the Ministry of Science and ICT (MSIT) of Republic of Korea.

### Availability of data and materials

The datasets used and/or analyzed during the current study are available from the corresponding author on reasonable request.

### Declarations

#### Competing interests

The authors declare that they have no competing interests.

Received: 30 March 2023 Accepted: 20 June 2023

Published online: 26 July 2023

### References

- Ryu HW, Lee SU, Lee SH, Song HH, Son TH, Kim YU, Yuk HJ, Ro HJ, Lee CK, Hong ST, Oh SR (2017) 3-Methoxy-catalposide inhibits inflammatory effects in lipopolysaccharide-stimulated RAW264.7 macrophages. *Cytokine* 91:57–64
- Lee KH, Woo JS, Kim JY, Lee CH, Yoo CG (2023) YPL-001 shows various beneficial effects against cigarette smoke extract-induced emphysema formation: anti-inflammatory, anti-oxidative, and anti-apoptotic effects. *Antioxidants* 12:15
- Oh SR, Lee MY, Ahn KS, Park BY, Kwon OK, Jung H, Lee JK, Kim DY, Lee SK, Kim JH, Lee HK (2006) Suppressive effect of verproside isolated from *Pseudolysimachion logifolium* on airway inflammation in a mouse model of allergic asthma. *Int Immunopharmacol* 6:978–986
- Lee KR, Choi J, Choi BK, Gu YM, Ryu HW, Oh SR, Lee HJ (2019) Picroside II isolated from *Pseudolysimachion rotundum* var. *subintegrum* inhibits glucocorticoid refractory serum amyloid A (SAA) expression and SAA-induced IL-33 secretion. *Molecules* 24:2020
- Lee CH, Ryu HW, Kim SH, Kim M, Oh SR, Ahn KS, Park JY (2020) Verminoside from *Pseudolysimachion rotundum* var. *subintegrum* sensitizes cisplatin-resistant cancer cells and suppresses metastatic growth of human breast cancer. *Sci Rep* 10:20337
- Liu S, Lou Y, Li Y, Zhang J, Li P, Yang B, Gu Q (2022) Review of phytochemical and nutritional characteristics and food applications of *Citrus* L. fruits. *Front Nutr* 9:968604
- Sánchez-Bermúdez M, del Pozo JC, Pernas M (2022) Effects of combined abiotic stresses related to climate change on root growth in crops. *Front Plant Sci* 13:918537
- Raza A, Razzaq A, Mehmood SS, Zou X, Zhang X, Lv Y, Xu J (2019) Impact of climate change on crops adaptation and strategies to tackle its outcome: a review. *Plants* 8:34
- Waqas MA, Kaya C, Riaz A, Farooq M, Nawaz I, Wilkes A, Li Y (2019) Potential mechanisms of abiotic stress tolerance in crop plants induced by thiourea. *Front Plant Sci* 10:1336
- Beteinakis S, Papachristodoulou A, Mikros E, Halabalaki M (2022) From sample preparation to NMR-based metabolic profiling in food commodities: the case of table olives. *Phytochem Anal* 33:83–93
- Kumar R, Bohra A, Pandey AK, Pandey MK, Kumar A (2017) Metabolomics for plant improvement: status and prospects. *Front Plant Sci* 8:1302



12. Lee HJ, Suh DH, Jung ES, Park HM, Jung GY, Do SG, Lee CH (2015) Metabolomics of *Lonicera caerulea* fruit during ripening and its relationship with color and antioxidant activity. *Food Res Int* 78:343–351
13. Liu J, Liu Y, Wang Y, Abozeid A, Zu YG, Zhang XN, Tang ZH (2017) GC-MS metabolomic analysis to reveal the metabolites and biological pathways involved in the developmental stages and tissue response of *Panax ginseng*. *Molecules* 22:496
14. Shin GR, Lee SM, Lee SR, Do SG, Shin EJ, Lee CH (2015) Maturity stage-specific metabolite profiling of *Cudrania tricuspidata* and its correlation with antioxidant activity. *Ind Crops Prod* 70:322–331
15. Xiao Q, Mu X, Liu J, Li B, Liu H, Zhang B, Xiao P (2022) Plant metabolomics: a new strategy and tool for quality evaluation of Chinese medicinal materials. *Chin Med* 17:45
16. Yuk HJ, Ryu HW, Kim DY, Park MH, Seo WD, Jeong SH, Oh SR (2019) Comparison of flavonoid and policosanol profiles in Korean winter-spinach (*Spinacia oleracea* L.) cultivated in different regions. *Food Chem* 279:202–208
17. Lu Q, Sun Y, Shu Y, Tan S, Yin L, Guo Y, Tang L (2016) HSCCC separation of the two iridoid glycosides and three phenolic compounds from *Veronica ciliata* and their *in vitro* antioxidant and anti-hepatocarcinoma activities. *Molecules* 21:1234
18. Feng SX, Yi B, Zhang M, Xu J, Lin H, Xu WT (2017) Iridoid glycosides from *Callicarpa nudiflora* hook. *Nat Prod Res* 31:181–189
19. Jensen SR, Gottfredsen CH, Harput US, Saracoglu I (2010) Chlorinated iridoid glycosides from *Veronica longifolia* and their antioxidant activity. *J Nat Prod* 73:1593–1596
20. Lee YN, Yoo JS, Shin DH, Ryoo BH, Ahn KS, Oh SR, Lee HK, Shin IS, Kim DY, Kwon OK, Song HH, Kim SH, Lee SU (2014) The composition comprising a purified extract isolated from *pseudolysimachion rotundum* var. *subintegrum* containing abundant amount of active ingredient or the compounds isolated therefrom, as an active ingredient for preventing or treating chronic obstructive pulmonary disease and the use thereof. Patent WO 2014/168413A1
21. Cho BO, Ryu HW, Jin CH, Choi DS, Kang SY, Kim DS, Byun MW, Jeong IY (2011) Blackberry extract attenuates oxidative stress through up-regulation of Nrf2-dependent antioxidant enzymes in carbon tetrachloride-treated rats. *J Agric Food Chem* 59:11442–11448
22. Lee BW, Lee JH, Gal SW, Moon YH, Park KH (2006) Selective ABTS radical-scavenging activity of prenylated flavonoids from *Cudrania tricuspidata*. *Biosci Biotechnol Biochem* 70:427–432
23. Lee SU, Lee SH, Ro HJ, Choi JH, Ryu HW, Kim MO, Yuk HJ, Lee JH, Hong ST, Oh SR (2018) Piscroside C inhibits TNF- $\alpha$ /NF- $\kappa$ B pathway by the suppression of PKC $\delta$  activity for TNF-RSC formation in human airway epithelial cells. *Phytomedicine* 40:148–157
24. Lee JW, Ji SH, Lee MK, Kim GS, Ahn YS, Ko HJ, Baek NI, Lee DY (2015) Metabolomics based on UPLC-QTOF/MS applied for the discrimination of *Cynanchum wilfordii* and *Cynanchum auriculatum*. *Metabolomics* 5:4
25. Hong JL, Qin XY, Shu P, Wu G, Wang Q, Qin MJ (2010) Analysis of catalpol derivatives by characteristic neutral losses using liquid chromatography combined with electrospray ionization multistage and time-of-flight mass spectrometry. *Rapid Commun Mass Spectrom* 24:2680–2686
26. Dinda B, Debnath S, Banik R (2011) Naturally occurring iridoids and secoiridoids. An updated review, part 4. *Chem Pharm Bull* 59:803–833
27. Kim MG, Hwang DK, Jeong HU, Ji HY, Oh SR, Lee YN, Yoo JS, Shin DH, Lee HS (2012) *In vitro* and *in vivo* metabolism of verproside in rats. *Molecules* 17:11990–12002
28. Kouda R, Yakushiji F (2020) Recent advances in iridoid chemistry: biosynthesis and chemical synthesis. *Chem Asian J* 15:3771–3783
29. Biere A, Marak HB, van Damme JMM (2004) Plant chemical defense against herbivores and pathogens: generalized defense or trade-offs? *Oecologia* 140:430–441
30. Leisner CP, Kamileen MO, Conway ME, O'Connor SE, Buell CR (2017) Differential iridoid production as revealed by a diversity panel of 84 cultivated and wild blueberry species. *PLoS ONE* 12:e0179417
31. Cho KM, Lee HY, Lee YM, Seo EY, Kim DH, Son KH, Lee JH, Cho DY, Lee JH (2022) Comparative assessment of compositional constituents and antioxidant effects in ginseng sprouts (*Panax ginseng*) through aging and fermentation processes. *LWT - Food Sci Technol* 164:113644
32. Kim DH, Yang WT, Cho KM, Lee JH (2020) Comparative analysis of isoflavone aglycones using microwave-assisted acid hydrolysis from soybean organs at different growth times and screening for their digestive enzyme inhibition and antioxidant properties. *Food Chem* 305:125462
33. Lee JH, Hwang CE, Son KS, Cho KM (2019) Comparisons of nutritional constituents in soybeans during solid state fermentation times and screening for their glucosidase enzymes and antioxidant properties. *Food Chem* 272:362–371
34. Lee JH, Cho YS (2021) Assessment of phenolic profiles from various organs in different species of perilla plant (*Perilla frutescens* (L.) Britt.) And their antioxidant and enzyme inhibitory potential. *Ind Crops Prod* 171:113914
35. Lee JH, Kim SC, Lee HY, Cho DY, Jung JG, Kang DW, Kang SS, Cho KM (2021) Changes in nutritional compositions of processed mountain-cultivated ginseng sprouts (*Panax ginseng*) and screening for their antioxidant and anti-inflammatory properties. *J Funct Foods* 86:104668
36. Li Y, Tang XX (2021) Abnormal airway mucus secretion induced by virus infection. *Front Immunol* 12:701443
37. Lee SG, Kwon SO (2021) Effects of inhibiting glycoprotein MUC5AC by seaweed *Ecklonia cava* extract in human airway epithelial cells. *Biomed Sci Lett* 27:334–339
38. Lee SR, Do SG, Kim SY, Kim JW, Jin YJ, Lee CH (2012) Mass spectrometry-based metabolite profiling and antioxidant activity of *Aloe vera* (*Aloe barbadensis* Miller) in different growth stages. *J Agric Food Chem* 60:11222–11228
39. Lee YN, Yoo JS, Shin DH, Ryoo BH, Ahn KS, Oh SR, Lee HK, Shin IS, Kim DY, Kwon OK, Song HH, Kim SH, Lee SU (2014) A purified extract isolated from *Pseudolysimachion rotundum* var. *subintegrum* containing abundant amount of catalpol derivatives, as an active ingredient for preventing or treating chronic obstructive pulmonary disease. Patent KR 10-2014-0122656

## Publisher's Note

Springer Nature remains neutral with regard to jurisdictional claims in published maps and institutional affiliations.

Submit your manuscript to a SpringerOpen® journal and benefit from:

- Convenient online submission
- Rigorous peer review
- Open access: articles freely available online
- High visibility within the field
- Retaining the copyright to your article

Submit your next manuscript at ► [springeropen.com](https://www.springeropen.com)